JOHANNES KEPLER
UNIVERSITY LINZ

Author

Tobias Grabner

Submitted at

Institute of Physical Chemistry and Linz Institute for Organic Solar Cells

Thesis Supervisor

a. Univ. Prof. Dr. Markus Scharber

Thesis Co-Supervisor

DI Katarina Gugujonović

September 2023

Integration of organic halide additives to a wide band-gap perovskite solar cell

Bachelor Thesis

to obtain the academic degree of

Bachelor of Science (BSc)

in the Bachelor's Program

Chemistry and Chemical Technology

JOHANNES KEPLER
UNIVERSITY LINZ

SWORN DECLARATION

I hereby declare that the thesis submitted is my own unaided work, that I have not used other than the sources indicated, and that all direct and indirect sources are acknowledged as references.

Linz, 17 September 2023

Acknowledgment

I would like to express my deepest gratitude to my supervisor DI Katarina Gugujonović for her guidance, and introduction to this highly interesting topic. Thanks for the big amount of time spent on discussions and always having an open ear for all my questions to lead me through this work.

Also, a big thanks go to Assoc. Prof. DI Dr. Markus Scharber, who supported me many times with practical tips for the conducted measurements.

My special thanks go to o.Univ. Prof. Mag. Dr. DDr. H.c. Niyazi Serdar Sariçiftçi, who encouraged me with his exciting lectures to dive deeper into the subjects of Physical Chemistry and gave me the opportunity to be a part of his team.

Big thank you to all the members of the LIOS group, who were helping me from the first day on and gave me such a warm welcome. The precious conversations and experiences within the group and the countless times of heartfully laughing with each other gave me a wonderful feeling to belong to this family.

Finally, I want to express my gratitude to my family, my friends, and especially my girlfriend for their unconditional support. When times are tough, you accept me, for who I am and always be the biggest boost for my motivation and self-awareness.

Thanks to all the people, that made this work possible!

Abstract

Perovskite solar cells have emerged as a promising alternative to traditional silicon-based photovoltaic technologies due to their remarkable efficiency, lower fabrication costs, and excellent material properties. In order, to yield increased performance in these devices, a special focus was laid over the past years on the development of wide-band gap perovskite solar cells with increased halide content. However, the instability of these perovskite materials remains a common challenge, hindering commercial availability. In this thesis 4-fluorobenzylammonium iodide, phenethylammonium iodide, and methylammonium iodide were implemented in a wide-band gap perovskite layer. Therefore, obtained 3D/2D heterostructure perovskites were characterized with measurements of current density-voltage-curves, external quantum efficiency, steady-state photoluminescence, and long-time stability by maximum power point tracking. The aim of this thesis is to underline the potential of perovskite heterostructures for increased stability and power conversion efficiency, as a matter of surface passivation and reduced deficiencies within the perovskite layer.

Kurzfassung

Perowskit-Solarzellen haben sich aufgrund ihrer bemerkenswerten Effizienz, geringeren Herstellungskosten und hervorragenden Materialeigenschaften als vielversprechende Alternative zu herkömmlichen Photovoltaiktechnologien auf Siliziumbasis erwiesen. Um die Leistung dieser Bauteile zu steigern, wurde in den letzten Jahren ein besonderer Schwerpunkt auf die Entwicklung von Perowskit-Solarzellen mit großer Bandlücke und erhöhtem Halogenidanteil gelegt. Allerdings stellt die Instabilität dieser Perowskitmaterialien ein häufiges Problem dar, das den kommerziellen Gebrauch erschwert. In dieser Arbeit wurden 4-Fluorobenzylammonium iodid, Phenethylammonium iodid und Methylammonium iodid in eine Perowskitschicht mit großer Bandlücke integriert. Die dadurch erhaltenen 3D/2D-Heterostruktur-Perowskite wurden mit Messungen wie Stromdichte-Spannungs-Kurven, externe Quanteneffizienz, Steady-State-Photolumineszenz und Langzeitstabilität mittels Maximum Power Point Tracking charakterisiert. Ziel dieser Arbeit ist es, das Potenzial von Perowskit-Heterostrukturen für eine erhöhte Stabilität und Leistungsumwandlungseffizienz durch Oberflächenpassivierung und verringerte Defekte innerhalb der Perowskitschicht hervorzuheben.

Table of Content

List of Abbreviations

BCP	Bathocuproine
CB	Chlorobenzene
DMF	Dimethylformamide
ETL	Electron transport layer
EtOH	Ethanol
FBAI	4-Fluorobenzyl ammonium iodide
FABr	Formamidinium bromide
HTL	Hole transport layer
IPA	Isopropyl alcohol
ITO	Indium tin oxide
MACl	Methylammonium chloride
MeO-2PACz	(2-(3,6-Dimethoxy-9H-carbazol-9-yl)ethyl)phosphonic acid
NMP	N-Methyl-2-pyrrolidine
$PC_{60}BM$	[6,6]-Phenyl-C_{61}-butyricacidmethylester
PCE	Power conversion efficiency
PEAI	Phenethylammonium iodide
PL	Photoluminescence
SEM	Scanning Electron Microscope

List of Figures

List of Tables

1. Introduction

Permanent population growth and a steadily industrial advancement increases the global demand for energy and drives the necessity of finding suitable strategies and methods for sustainable and efficient energy generation and storage. Over the last decades, big investments were put into a large variety of renewable energy sources, such as wind, geothermal or hydropower energy, respectively. However, besides these already long applied energy sources, newer technologies have been developed over the last centuries, including solar cells as a promising future. [1] Although the photovoltaic effect was discovered much earlier in 1839 and first solar cells were developed around 1883 by American inventor Charles Fritts, it took more than half a century, to produce the first useful devices. 1954, Bell Laboratories, seated in Murray Hill, New Jersey, developed the first practical solar cell from silicon, setting a milestone as a new energy source. [2]

Nowadays, solar cells have gained high status for several reasons. First, the sun naturally emits an enormous amount of energy, reaching the earth and representing the most abundant form of renewable energy. One of the most important aspects is being eco-friendly, as apart from the manufacturing process, solar cells have no CO_2 emissions. Today's global photovoltaic market is dominated by silicon based cells, reaching an incredible power conversion efficiency (PCE) of up to 26 % with a low price of around 0.03 – 0.06 € per kWh. [1, 3] However, constant research and development on photovoltaic devices is aiming for even further increase in performance, while lowering costs. Next to organic solar cells, that gained high importance over the last decades, a new material class was introduced in 2009 with the discovery of the semiconducting properties of the so-called perovskites. [4]

1.1. Perovskites

Solar cells that consist of perovskites as photoactive material are based on a blend of organic and inorganic lead halides and are therefore referred to as hybrid organic-inorganic lead halide perovskites (OIHP). According to figure 1, the perovskite material class can be described as a cubic-octahedral crystal structure in the composition ABX_3. The atom A is representing either an organic cation, such as formamidinium (FA) and in smaller quantity some metal cation like Cs^+, as used in this thesis. The B atom is the divalent Pb^{2+}, while X is denoting the halides, like Br^-, I^- and Cl^-.

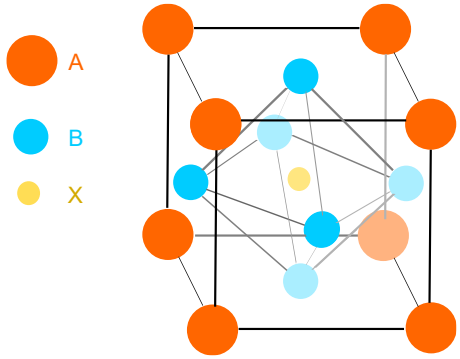

Figure 1: Structure of an organic-inorganic lead halide perovskite with general composition ABX_3.

Even tough, perovskite solar cells have not been established yet in big commercial use, high performances of up to 26 % [5] on lab scale experiments have shown, that perovskites have a promising future as a photoactive material. Properties such as high light absorptivity, and a tuneable band gap underlines the potential behind perovskite solar cells. Most important advantage is the expected reduced costs, as the OIHPs can be fabricated with less energy-intensive processes compared to silicon solar cells. [4]

1.2. Function of a Perovskite Solar Cell

When the photoactive perovskite layer is exposed to light, photons can be absorbed. In affect a so-called exciton is formed. Excitons can be described as a bound electron-hole pair. While the excited electron moves towards the conducting band, a positive charge carrier remains in the valence band, which is referred to as hole. [6] The exciton formation is dependent on the band gap. The band gap refers to the energy difference between the highest energetic state in the valence band and the lowest one in the conducting band in semiconducting materials. The exciton formation is only possible, when the photon absorbed by the perovskite layer has a higher energy than this band gap. For conventional silicon solar cells, the band gap energy is 1.1 eV, allowing the absorption of a broad part of the solar spectrum. When the absorbed photons exceed this band gap, energy losses due to the excess of energy result.

The band gap can be controlled over the composition of the perovskite. One of the most prominent examples that has established in related research are perovskites based on methylammonium lead iodide (MAPI). For comparison with silicon solar cells, MAPI perovskites have a band gap of around 1.6 eV. [7] Over the last years, the development of wide-band gap solar cells, with around 1.5 – 2.5 eV gained on importance. The higher band gap covers the absorption of photons with shorter wavelength. This enables the application in areas, where higher voltages are required. Furthermore, wide-band gap perovskites have big potential for the application in tandem solar cells, where higher power conversion can be achieved by combining photoactive materials with varying band gaps. [8] In this thesis, a well-established wide-band gap perovskite recipe from literature [9] was used, which is described in detail in chapter 2.2.

In figure 2, the scheme of charge generation in the OIHPs is drawn. In step 1, the absorption of incident photons leads to the exciton formation. Step 2 shows the charge transfer of electron and hole into the respective charge transport layer. Therefore, electron and hole separate by transfer into the electron transport layer (ETL) and the hole transport layer (HTL), respectively. In the following step 3, the charge extraction proceeds, where the electrons are transferred over the ETL towards the cathode, while the holes are transported over the HTL further to the anode. [10]

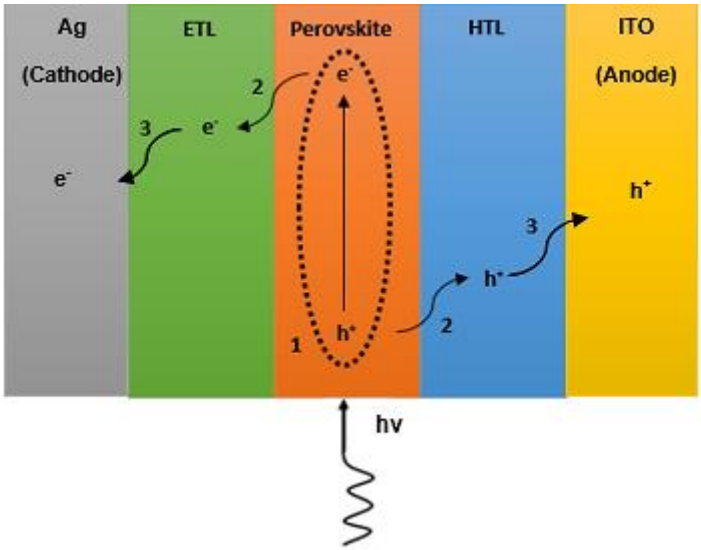

Figure 2: Illustration of the photo-induced processes in a perovskite solar cell: **1)** exciton formation by photon absorption, **2)** charge transfer, **3)** charge extraction at the electrodes.

1.3. Efficiency of a Solar Cell

The main tool for the determination of the efficiency of the perovskite solar cells is the current density-voltage (I-V) measurement. The characteristic I-V curves show the relationship between current and voltage. In figure 3 an example for a typical I-V curve is depicted. [11]

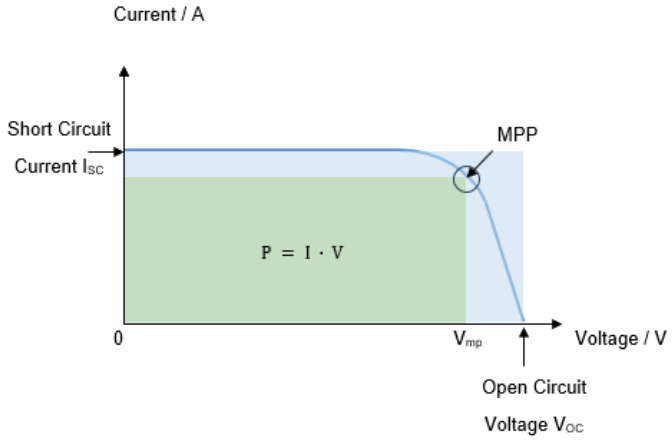

Figure 3: A typical current density-voltage curve of a solar cell under illumination.

During the I-V measurement, different voltages are applied, and the corresponding current is recorded. The open circuit voltage V_{OC} refers to the voltage when no current is present. On the other hand, the short circuit current I_{SC} is the maximum current occurring, when no voltage is applied. According to Eq. 1, the power output of a single solar cell can be described as the product of current and voltage. [11]

$$P = I \cdot V \tag{1}$$

Hence, each cell has a maximum power output, which is referred to as maximum power point MPP.

Another important parameter for the determination of the performance is the fill factor FF. This factor describes the ratio of the maximum power of a solar cell to the product of V_{OC} and J_{SC}, as shown in Eq. 2. [11]

$$\mathrm{FF} = \frac{P_{max}}{V_{OC} \cdot I_{SC}} \tag{2}$$

In figure 3, this would be the ratio of green to blue area. The bigger the fill factor, the higher the power output. Finally, the Power conversion efficiency of the solar cell can be calculated according to Eq. 3. [12]

$$\mathrm{PCE} = \frac{\mathrm{FF} \cdot V_{OC} \cdot I_{SC}}{P_{in}} = \frac{P_{max}}{P_{in}} \tag{3}$$

1.4. Imperfections and Passivation in Perovskite Solar Cells

As the photoactive perovskite layer in OIHP represents a complex structure, deficiencies and imperfections in the crystal lattice can be expected. Such imperfections may origin from impurities in the raw materials for the precursor solution. Another possibility are grain boundaries and defects on the surface of the film or the formation of lead clusters due to evaporation of the surrounding organic cations or halides. Those defects could negatively influence the performance of the device, in respect to V_{OC}, J_{SC}, FF and PCE. [13] Several methods have been developed for efficiently reducing occurring imperfections, including the implementation of additives into the perovskite composition. As the materials used for OIHPs are of ionic nature, mechanisms for passivating defects would include coordinative bonding of Lewis acids or -bases or also ionic bonding, such as introducing bulky cations into the structure.[14] In this thesis, 4-Fluorobenzylammonium iodide (FBAI) and Phenethylammonium iodide (PEAI) were added to a wide-band gap recipe. Their structure is depicted in figure 4a and 4b. With applying these bulky cations so-called 3D/2D perovskite heterostructures are formed. These heterostructures promise to yield very efficient surface passivation and increase the efficiency of the solar cell. [15] Another important aspect for providing high efficiency solar cells is the orientation of the crystal growth of the 2D perovskite layer. Methylammonium chloride (MACl) is an organic compound, reported in several papers as an efficient additive to control a vertical crystal growth and leading to an improved surface of the 3D/2D heterostructure perovskite layers. [15]Figure 4 shows a classical 3D/2D heterostructure perovskite.

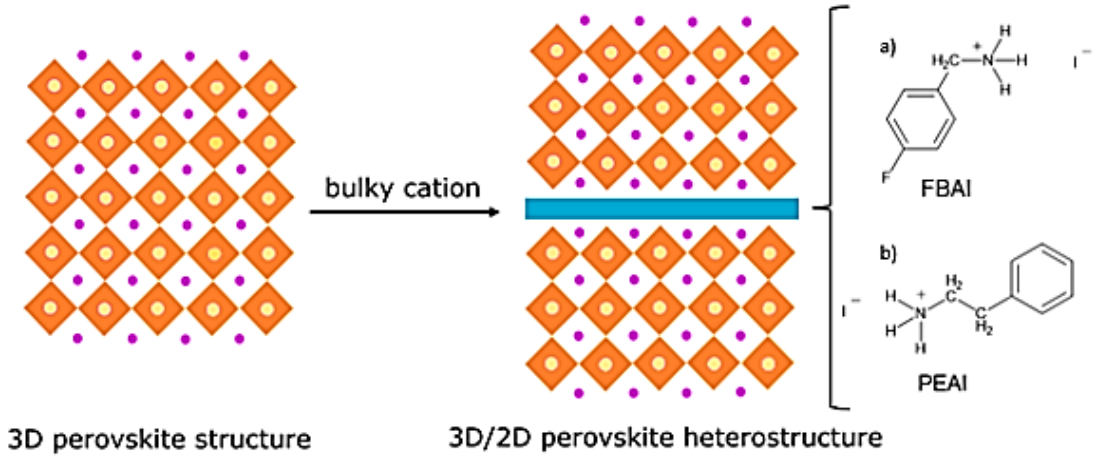

Figure 4: 3D/2D perovskite heterostructure, formed by the bulky cations **a)** 4-Fluorobenzylammonium iodide (FBAI) or **b)** Phenethylammonium iodide (PEAI).

The 2D perovskite layer consists of the bulky cation, causing the formation of stacked monolayers of lead halides. According to [16], the chemical formula for a mixed 3D/2D perovskite is denoted as $R_2A_{n-1}B_nX_{3n+1}$, whereas A is defined once again by FA or Cs^+, B as Pb^{2+} and X as the halide anions, Br^-, Cl^- or I^-. R is the bulky organic cation. The factor n describes the stoichiometric ratio between 3D perovskite arrangements and the 2D cation. A value of n=2 would therefore mean that after each 2 crystal layers of a classical 3D perovskite, one layer of 2D perovskite is formed. [16] Despite their positive effects on passivation of the perovskite surface, 2D perovskite show some properties that can limit the efficiency of the devices. The bulky cation can cause difficulties for the charge transport; While the conductivity is higher within the 3D perovskite, the 2D layer has insulating properties and hinders the charge transfer towards the electrodes. Therefore, the used amounts of FBAI, PEAI and MACl need to be optimized in order to prevent bigger losses in current. [24]

2. Experimental

2.1. Materials

Table 1: Used materials, supplier, purity, and abbreviation.

Material	Supplier	Purity / %	Abbreviation
Bathocuproine	Sensient Imaging	n/a	BCP
Caesium bromide	Alfa Aesar	99.9	CsBr
Chlorobenzene	Alfa Aesar	99.8	CB
Chloroform	Sigma Aldrich	>99.5	$CHCl_3$
Ethanol	VWR Chemicals	>99.8	EtOH
Formamidinium bromide	-	-	FABr
4-Fluorobenzyl ammonium iodide	TCI Chemicals	>98	FBAI
Hydrochloric acid	VWR Chemicals	37	HCl
Indium tin oxide coated glass	Xinayan Hongkong	-	ITO
Isopropyl alcohol	Merck	100	IPA
Lead(II) bromide	Alfa Aesar	>98	$PbBr_2$
Lead(II) iodide	Alfa Aesar	99.9985	PbI_2
Methanol	VWR Chemicals	>99.8	MeOH
Methylammonium chloride	Greatcellsolar	99.99	MACl
(2-(3,6-Dimethoxy-9H-carbazol-9-yl)ethyl)phosphonic acid	TCI Chemicals	>98.0	MeO-2PACz
N,N-Dimethylformamide	Sigma Aldrich	99.8	DMF
N-Methyl-2-pyrrolidine	Alfa Aesar	99.5	NMP
[6,6]-Phenyl-C_{61}-butyricacidmethylester	Solenne	99	$PC_{60}BM$
Phenethylammonium iodide	Sigma Aldrich	98	PEAI
Silver	chemPUR	99.999	Ag
Thiourea	Sigma Aldrich	99	-
Toluene	VWR Chemicals	>99.0	-

2.2. Solution Preparation

For the preparation of 2 mL of a 1.08 M wide-bandgap perovskite precursor solution with a composition of $FA_{0.8}Cs_{0.2}Pb(I_{0.5}Br_{0.5})_3$, following amounts were used according to table 2.

Table 2: Materials and amounts used for 2 mL of a 1.08 M perovskite precursor solution.

Material	mass / mg
Lead (II) iodide	691.51
Lead (II) bromide	183.50
Caesium bromide	85.12
Formamidinium bromide	199.95

The solid mixture was dissolved in 1600 µL dimethylformamide (DMF) and 400 µL N-methyl-2-pyrrolidine (NMP) and stirred overnight. Afterwards, the solution was filtered over a 0.45 µm PTFE filter. A defined volume of 1800 µL was transferred to another vial and 1 vol.-% of Thiourea (100 mg mL^{-1} in DMF) was added before use.

For the HTL, the material MeO-2Pacz was used. The solution was prepared with a concentration of 0.3 mg mL^{-1} in ethanol. As ETL, $PC_{60}BM$ was applied. A solution of 20 mg mL^{-1} was prepared in a solvent mixture of chloroform and chlorobenzene (CB) in a ratio 3:1. As a buffer layer between the electrode and the ETL, bathocuproine (BCP) was used. The BCP solution was prepared in a concentration of 0.5 mg mL^{-1} in ethanol. The respective structures of the components are shown in figure 5.

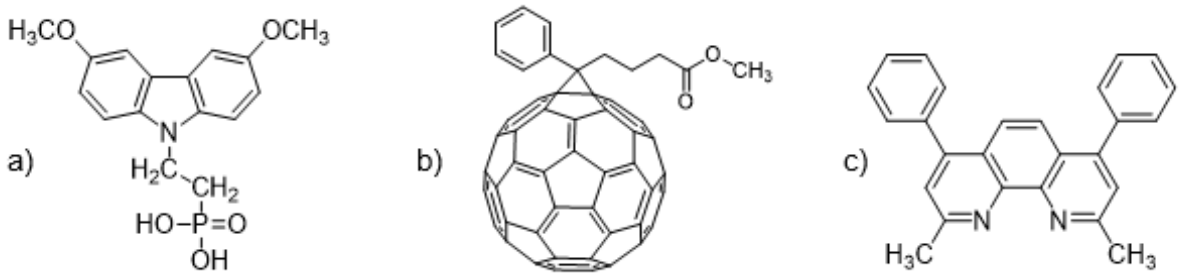

Figure 5: Structures of ***a)*** (2-(3,6-Dimethoxy-9H-carbazol-9-yl)ethyl)phosphonic acid (MeO-2PACz), ***b)*** [6,6]-Phenyl-C*61*-butyricacidmethylester ($PC_{60}BM$) and ***c)*** Bathocuproine (BCP)

2.3. Device Fabrication

The solar cell substrates were prepared from indium tin oxide (ITO) coated glass. Therefore, stripes of 2.5 cm width were cut and cleaned with toluene by using cleaning wipes. The middle part was covered with PVC tape, such that around 0.5 cm were kept free at both sides. The ITO was etched with concentrated hydrochloric acid for 15 min. Afterwards the substrate was washed with deionized H_2O. After removing the PVC tape, another cleaning step with toluene on cleaning wipes was performed. The stripes were then cut into $2.5 \times 2.5\ cm^2$ pieces and further cleaned in Hellmanex solution in an ultrasonic bath at 80°C. After 30 minutes, the substrates were washed several times with deionized water, before storing them in isopropyl alcohol (IPA). For the Photoluminescence (PL) and Transmission measurements, the same procedure was conducted with a microscope glass slide, instead of ITO glass. Using different spin-coating programs (see **Table *4***), the HTL, perovskite layer, ETL and BCP buffer were processed as thin films onto the ITO substrate, yielding a solar cell device according to figure 6.

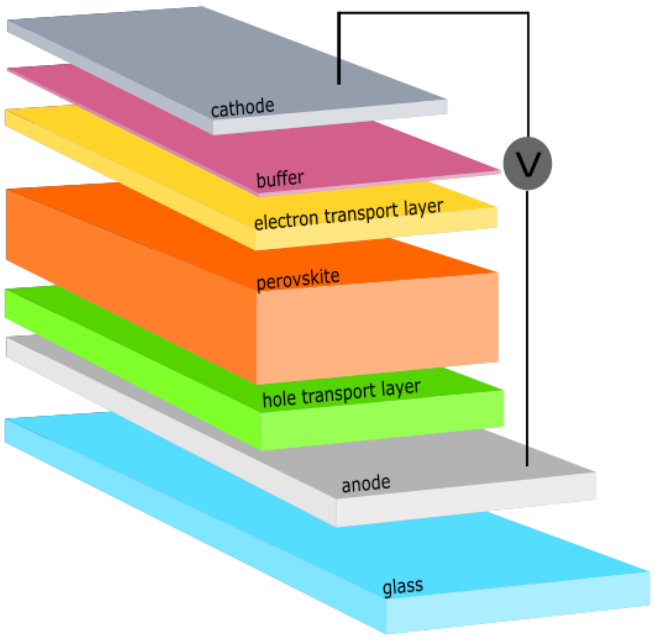

Figure 6: A perovskite solar cell with the following upward order: Anode | hole transport layer (HTL) | perovskite | electron transport layer (ETL) | buffer layer (BCP) | cathode

For the generation of the 3D/2D heterostructure perovskites, the bulky cations FBAI and PEAI as well as MACl were used as additives. In course of the optimization process, various amounts of additives and additive integration methods were tested. The applied concentrations of each additive and the type of how they were introduced to the perovskite are listed in table 3.

Table 3: Used Additives, concentrations, and application type for the perovskite layer.

Material	c / mg mL^{-1}	Type
MACl	2.50	Direct
	3.75	Direct
	5.00	Direct
FBAI	0.014 (n = 20)	Direct
	0.039 (n = 7)	Direct
	0.055 (n = 5)	Direct
	0.25	Extra layer
	0.50	Extra layer
PEAI	0.021 (n = 13)	Direct
	0.038 (n = 7)	Direct
	0.25	Extra layer
	0.50	Extra layer
	1.00	Extra layer

“Direct” type denotes that the additive was added to the perovskite precursor mixture, before dissolving in DMF and NMP. In an “extra layer” type, a solution of the additive in IPA was prepared separately. This solution was then spin-coated on top of the perovskite layer. As explained in section 1.5, the n denotes the stoichiometric ratio of 3D perovskite structure to 2D additive, meaning that after every nth crystal plane of 3D perovskite, one layer of 2D perovskite with the respective additive is formed. Figure 7 shows a schematic illustration of the two application types.

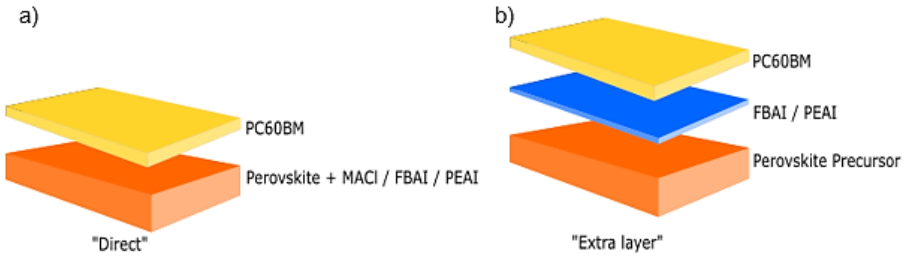

Figure 7: Additive application either as **a)** direct inclusion or **b)** extra layer

The parameters for the spin program, the annealing process, and the solvents used for patterning are summarized in table 4. Annealing on a heating plate was performed for HTL, perovskite, and additive layer. Patterning of the substrate is required to allow contact between the ITO and the Ag electrode, which will be lastly deposited on top. For the $PC_{60}BM$ electron transport layer, and the BCP buffer layer, no annealing was applied. Furthermore, patterning of $PC_{60}BM$ was done after BCP coating using CB as solvent. In case of the additive application as extra layer, the optimized parameters for FBAI and PEAI are listed in table 4. MACl is directly included in the perovskite layer.

Table 4: Optimized Spin coating programs for thin film deposition, Annealing parameters, and Patterning solvents.

Material	*c* / mg mL^{-1}	Spin Coating			Annealing		Patterning
		Speed rpm	Ramp rpm s^{-1}	Time s	Temperature °C	Time min	Solvent
MeO-2PACz	0.3	50	2	26	100	10	MeOH
		50	1	1			
Perovskite	1.08	8	1	1	65	2	DMF
		67	2	58	100	10	
FBAI / PEAI	0.25	8	1	1	100	10	IPA
		67	2	58			
$PC_{60}BM$	20	22	2	16	-	-	-
		33	2	15			
BCP	0.5	67	2	26	-	-	CB
		67	1	1			

Before the deposition of the perovskite layer, 200 µL MeOH were dropped onto the substrate (200 µL s^{-1}), 20 seconds before end of the perovskite spin coating program, according to table 4. Immediately after the end of the program, 180 µL of the perovskite solution were pipetted to cover the entire substrate. After starting the spin program, 200 µL Chlorobenzene (CB) were applied as an antisolvent 15 seconds after the start of the spin coater. For the cathode, silver contacts were evaporated on top of the solar cell using the Edwards Auto 500 vacuum evaporator. The samples were placed in a mask to provide a specific pattern for the contacts. Under a high vacuum, Ag was deposited on the surface of the substrate with a layer thickness of 100 nm.

2.4. Current density-Voltage (I-V)

The Current density-voltage characterization (I-V) was performed under AM1.5G illumination, using a Xenon arc lamp from LOT-Quantum Design. First, the light intensity of this “Sun-Simulator” was determined by a calibrated silicon solar cell (Mencke & Tegtmeyer). Then the solar cells are measured using a Keithley 2401 Source Meter and a voltage from -0.5 to 1.5 V.

2.5. External Quantum Efficiency (EQE)

For the external quantum efficiency measurement (EQE), a reference spectrum with a silicon photodiode from Hamamatsu (S2281) was recorded. A xenon arc lamp served as light source and a grating monochromator (Corner Stone 130 1/8 m) was used. For current detection, a potentiostat (Jaissle 1002 T-NC) with a lock-in amplifier (Stanford Research system SR830 DSP) was used. The current was recorded for each sample over a range of 350-800 nm. From the detected current, the EQE was calculated for each wavelength.

2.6. Maximum Power Point tracking (MPP)

For the MPP tracking, a halogen lamp was used as light source. The substrate was positioned under the lamp, and an I-V curve was recorded first by using a Keithley 2401 Source Meter. After adjusting the light intensity of the lamp to approximately 1 sun, the MPP-tracking tool was started. Measurements were conducted for 70 hours on each substrate.

2.7. Transmittance

The Transmittance *T* of the glass/MeO-2PACz/Perovskite substrates was measured with a double beam UV/Vis/NIR spectrometer (Perkin Elmer Lambda 1050). The signal detection was done by an InGaAs detector and a PS detector over a wavelength range of 350 nm - 1000 nm.

2.8. Steady-state Photoluminescence (PL)

For the photoluminescence measurement (PL) the glass/MeO-2PACz/perovskite substrates were illuminated by a laser (Coherent Obis, 405 nm excitation wavelength, 4.78 mW power). Two long-pass filters (420 nm) were used for the emitted light, before passing the monochromator (Shamrock 303i, Andor Technology). A charge-coupled device (CCD) camera (iDus 420, Andor Technology) was used to detect the emitted light. As reference, a microscope glass slide was measured.

2.9. Scanning Electron Microscopy (SEM)

Scanning electron microscopy (SEM) was performed on glass/ITO/MeO-2PACz/perovskite substrates using an acceleration voltage of 7 keV on the JEOL JSM-6360 LV microscope. Imaging of the sample was provided by the Bruker Nano X-Flash detector.

3. Results and Discussion

The aim of this thesis was to implement several additives to a wide band gap perovskite with the composition $FA_{0.8}Cs_{0.2}Pb(I_{1-x}Br_x)_3$. The additives were reported to cause passivation of defects and improves the charge carrier formation and mobility …[14]. MACl, which was directly added to the precursor, targets an improved crystal growth [15]. Accordingly, the concentration plays a major role for the crystallization process of the perovskite layer.

3.1. Current density-Voltage characterization (I-V)

In general, the cells were measured in forward direction “fwd” from -0.5 - 1.5 V and in reverse “rvs” from 1.5 - -0.5 V. The given numbers in the following tables represent the values for the cell with highest efficiency, while in brackets the average value out of n measured cells and the standard deviation is noted. Investigating the effect of MACl on the perovskite layer, following results for the devices with different MACl concentration are listed in table 5.

Table 5: Current density - voltage measurements for perovskite solar cells with different concentrations of Methylammonium chloride (MACl).

ρ_{MACl} / mg mL^{-1}	Scan	V_{OC} / V	J_{SC} / mA cm^{-2}	FF / %	PCE / %	n
w/o	fwd	1.15 (1.13 ± 0.02)	15.4 (13.9 ± 0.8)	76 (72 ± 4)	12.5 (11.1 ± 1.0)	22
	rvs	1.15 (1.13 ± 0.02)	15.5 (13.9 ± 0.8)	77 (72 ± 4)	12.9 (11.3 ± 1.1)	22
2.5	fwd	1.24 (1.19 ± 0.04)	15.2 (13.6 ± 0.9)	75 (71 ± 3)	12.6 (12.3 ± 0.6)	27
	rvs	1.24 (1.20 ± 0.03)	15.3 (13.6 ± 0.9)	79 (73 ± 4)	13.0 (12.4 ± 0.8)	27
3.75	fwd	1.22 (1.16 ± 0.04)	18.3 (14.7 ± 1.5)	75 (71 ± 2)	15.1 (12.5 ± 1.3)	31
	rvs	1.21 (1.17 ± 0.03)	18.5 (14.7 ± 1.5)	79 (74 ± 3)	15.5 (12.5 ± 1.0)	31
5.0	fwd	1.08 (1.06 ± 0.02)	8.8 (6.32 ± 2.1)	66 (62 ± 4)	5.3 (4.1 ± 1.1)	15
	rvs	1.08 (1.05 ± 0.03)	8.6 (6.30 ± 2.1)	68 (73 ± 3)	5.6 (4.8 ± 0.8)	15

From table 5, the following figure 8 can be deduced, showing an overview of the average performance of the perovskite solar cells with MACl.

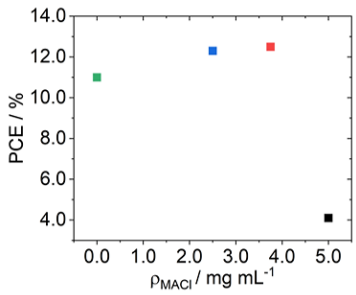

Figure 8: Power conversion efficiency (PCE) dependent on the concentration of methylammonium chloride (MACl).

This plot shows that a performance increase is just valid for a small range in concentration. Addition of 2.5 - 3.75 mg mL^{-1} MACl could increase the PCE from an average 11.2 % to approximately 11.9 - 12.2 %. Increasing the concentration further to 5.0 mg mL^{-1} MACl, appeared to lower the PCE to around 4.5 %. As already mentioned in chapter 1.4, additives used for heterostructures in perovskites do not only show passivating effects but are also known to be insulating. This significantly reduces the current and therefore also the PCE, which is coherent with the measured results. [24] Referring to the results of the I-V-measurement, the best performance was yielded with a concentration of 3.75 mg mL^{-1} MACl. Further devices were therefore produced with this concentration.

For the 3D/2D heterostructure perovskites the additives FBAI and PEAI were applied in two different ways, according to 2.3. Devices, that included PEAI or FBAI directly in the perovskite layer showed inconsiderable results in any concentration. As V_{OC} and J_{SC} are very low, no measurable PCE can be obtained. Hence, following tables 6 and 7 summarize only the results for the devices with an extra layer of FBAI and PEAI, respectively.

Table 6: Current density - voltage measurements for perovskite solar cells with different concentrations of 4-fluorobenzylammonium iodide (FBAI).

ρ_{FBAI} / mg mL^{-1}	Scan	V_{OC} / V	J_{SC} / mA cm^{-2}	FF / %	PCE / %	n
w/o	fwd	1.26 (1.24 ± 0.01)	14.1 (12.0 ± 1.1)	79 (72 ± 9)	13.3 (10.9 ± 2.0)	31
	rvs	1.25 (1.23 ± 0.01)	14.3 (12.1 ± 1.2)	79 (71 ± 8)	13.2 (10.7 ± 1.9)	31
0.25	fwd	1.24 (1.19 ± 0.04)	15.2 (13.6 ± 0.9)	75 (71 ± 3)	12.6 (11.7 ± 0.6)	27
	rvs	1.24 (1.20 ± 0.03)	15.3 (13.6 ± 0.9)	79 (73 ± 4)	13.0 (12.1 ± 0.8)	27

Table 6: Current density - voltage measurements for perovskite solar cells with different concentrations of 4-fluorobenzylammonium iodide (FBAI).

0.50	fwd	1.21 (1.14 ± 0.09)	13.1 (11.6 ± 1.6)	76 (55 ± 15)	12.4 (7.74 ± 3.2)	7
	rvs	1.22 (1.15 ± 0.08)	13.1 (11.8 ± 1.5)	75 (57 ± 13)	12.1 (8.20 ± 2.9)	7

Table 7: Current density - voltage measurements for perovskite solar cells with different concentrations of Phenethylammonium iodide (PEAI).

ρ_{PEAI} / mg mL^{-1}	Scan	V_{OC} / V	J_{SC} / mA cm^{-2}	FF / %	PCE / %	n
w/o	fwd	1.24 (1.19 ± 0.04)	15.2 (13.6 ± 0.9)	75 (71 ± 3)	12.6 (11.7 ± 0.6)	27
	rvs	1.24 (1.20 ± 0.03)	15.3 (13.6 ± 0.9)	79 (73 ± 4)	13.0 (11.5 ± 0.7)	27
0.25	fwd	1.25 (1.23 ± 0.01)	13.9 (12.1 ± 1.0)	80 (74 ± 4)	13.3 (11.1 ± 0.9)	16
	rvs	1.24 (1.22 ± 0.01)	13.8 (12.1 ± 1.0)	76 (73 ± 2)	12.1 (10.8 ± 0.8)	16
0.50	fwd	1.22 (1.21 ± 0.02)	13.6 (13.0 ± 0.5)	73 (69 ± 3)	12.4 (11.2 ± 0.9)	7
	rvs	1.21 (1.20 ± 0.02)	13.5 (12.9 ± 0.6)	70 (66 ± 2)	11.7 (10.6 ± 0.8)	7
1.00	fwd	1.25 (1.24 ± 0.01)	13.1 (12.7 ± 0.3)	77 (73 ± 4)	12.3 (10.4 ± 0.8)	8
	rvs	1.25 (1.22 ± 0.01)	13.1 (12.7 ± 0.3)	79 (73 ± 4)	12.0 (10.4 ± 0.7)	8

In the following figure 9a, the efficiency of solar cells with different FBAI concentrations are plotted. The best efficiency was achieved with a concentration of 0.25 mg mL^{-1}, yielding a PCE of around 11.7 %. Other devices with 0.5 mg mL^{-1} were produced, yielding a significant lower PCE of only 8.7 %. As expected from literature [24], the insulating properties of the organic material hinders the charge transport at the interface between the perovskite and the electron transport layer $PC_{60}BM$. [18] For comparison, solar cells without additive yield a PCE of about 11.0 %. Further devices with FBAI were therefore processed with the optimum concentration of 0.25 mg mL^{-1}.

In contrast to FBAI, the PEAI additive could not contribute in any tested concentration to an improvement in PCE, as seen in figure 9b. However, in order to check for improved stability, as expected from literature [15], further devices with PEAI were produced with a concentration of 0.25 mg mL^{-1}.

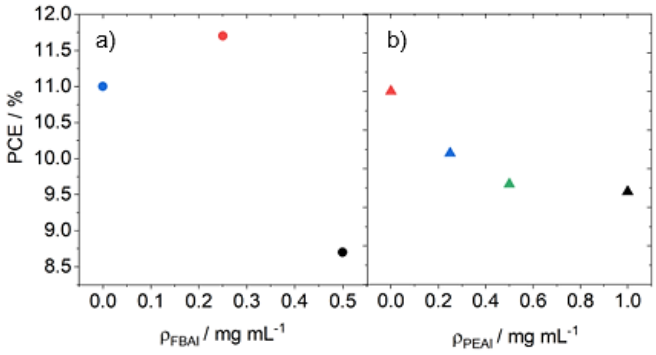

Figure 9: Power conversion efficiency (PCE) dependent on the concentration of **a)** 4-Fluorobenzylammonium iodide (FBAI) and **b)** Phenethylammonium iodide (PEAI).

Figure 10 shows the results for final processed perovskite solar cells with optimized composition, corresponding to the values listed in table 8. For evaluation, only cells with an FF of > 65 % were taken into consideration.

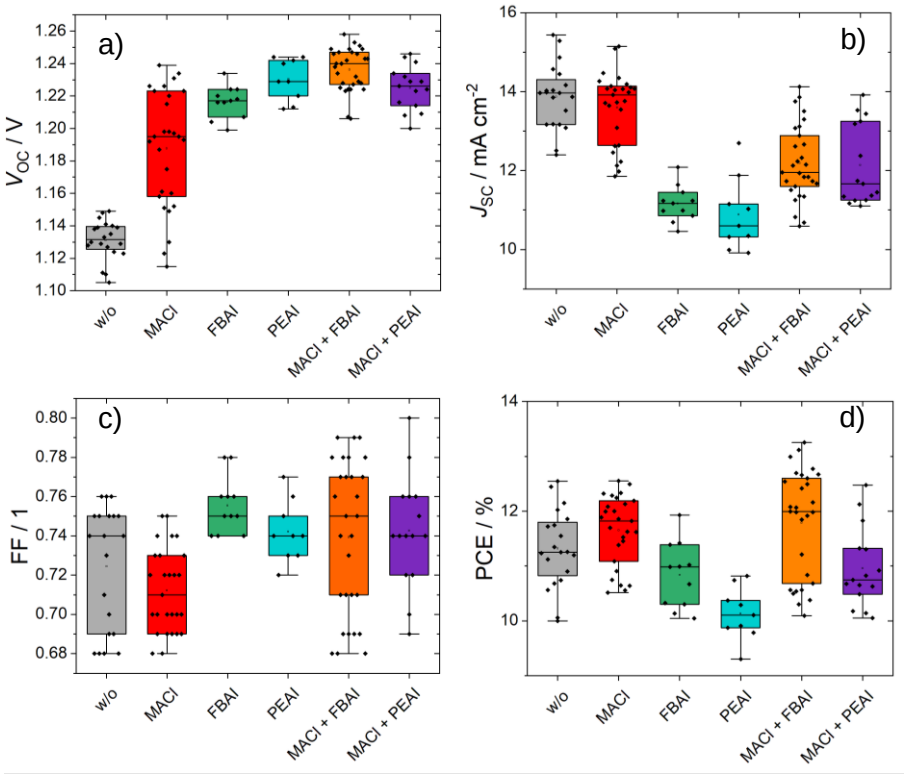

Figure 10: Box plots of solar cell parameters extracted from current density-voltage measurements of perovskite solar cells with different additives: **a)** Open circuit voltage (V_{OC}), **b)** Short circuit current (J_{SC}) / mA cm^{-2}, **c)** Fill factor (FF) and **d)** Power conversion efficiency (PCE).

Table 8: Current density - voltage measurements of perovskite solar cells with the optimized additive concentration.

$\rho_{Additive}$ / mg mL^{-1}	Scan	V_{OC} / V	J_{SC} / mA cm^{-2}	FF / %	PCE / %	n
w/o	fwd	1.15 (1.13 ± 0.01)	15.4 (13.9 ± 0.8)	76 (72 ± 3)	12.6 (11.3 ± 0.7)	22
	rvs	1.14 (1.13 ± 0.02)	15.5 (13.9 ± 0.8)	77 (72 ± 4)	12.6 (11.3 ± 0.7)	22
MACl	fwd	1.24 (1.19 ± 0.04)	15.2 (13.6 ± 0.9)	75 (71 ± 2)	12.6 (11.7 ± 1.0)	27
3.75	rvs	1.24 (1.18 ± 0.03)	14.9 (13.7 ± 1.5)	79 (74 ± 3)	12.5 (11.7 ± 0.9)	27
FBAI	fwd	1.24 (1.22 ± 0.01)	12.1 (11.2 ± 0.6)	78 (76 ± 2)	11.9 (11.0 ± 0.7)	11
0.25	rvs	1.24 (1.21 ± 0.03)	11.3 (10.6 ± 0.9)	79 (73 ± 4)	13.0 (11.0 ± 0.8)	11
PEAI	fwd	1.24 (1.23 ± 0.04)	12.7 (11.1 ± 1.0)	77 (74 ± 2)	10.8 (10.2 ± 0.6)	27
0.25	rvs	1.24 (1.22 ± 0.03)	12.5 (11.3 ± 1.0)	76 (73 ± 4)	10.6 (10.2 ±0.7)	27
MACl + FBAI	fwd	1.26 (1.24 ± 0.04)	14.1 (12.2 ± 1.0)	75 (74 ± 3)	13.3 (11.9 ± 0.6)	27
3.75 / 0.25	rvs	1.25 (1.25 ± 0.03)	14.3 (12.3 ± 0.9)	74 (73 ± 4)	12.5 (11.9 ± 0.7)	27
MACl + PEAI	fwd	1.25 (1.22 ± 0.01)	13.9 (12.1 ± 1.0)	80 (74 ± 3)	12.5 (11.0 ± 0.7)	27
3.75 / 0.25	rvs	1.24 (1.22 ± 0.02)	13.8 (12.3 ± 1.0)	79 (73 ± 4)	12.4 (11.0 ± 0.7)	27

According to chapter 1.4, bulky cations help the passivation of local imperfections in the perovskite thin film at the surface, and may lead to an improvement of the device parameters. [14] This passivating effect can be confirmed by comparison of the V_{OC} from figure 9a. The measured V_{OC} could be increased for all devices upon addition of additives. The highest V_{OC} with 1.25 V was measured with addition of MACl + FBAI, yielding a 3D/2D heterostructure perovskite. When comparing this value with the V_{OC} of 1.22 V for FBAI, it can be deduced that MACl further increase the efficiency of the heterostructure.

An opposite relation was obtained for the J_{SC}. While the devices with standard perovskite composition showed an average J_{SC} of around 14 mA cm^{-2}, the measured current dropped significantly upon addition of FBAI and PEAI to ≤ 12 mA cm^{-2}. As already pointed out, this is due to the insulating properties, which hinder the charge transport to the electrodes. [13]

Considering the fill factor FF, no significant deviations can be seen. To summarize all devices, an average FF of 74 % was reached, while the maximum of 76 % was obtained for the FBAI additive.

A combination of the discussed parameters results finally in the PCE of the solar cells, whereas no clear trend can be derived. For the most additives, no efficiency improvement could be achieved, when comparing to an average PCE of 11.3 % in devices without additive. However, the combination of MACl with FBAI appeared to have the best results. With a maximum achieved PCE of 13.3 % and on average 11.9 %, the improvement in performance by the application of MACl in 3D/2D heterostructure perovskites can be underlined.

3.1. External Quantum Efficiency (EQE)

The EQE is another characteristic parameter for the performance of a solar cell. It describes the ratio between the number of electrons generated and the number of incident photons, as a function of the wavelength λ. [19]

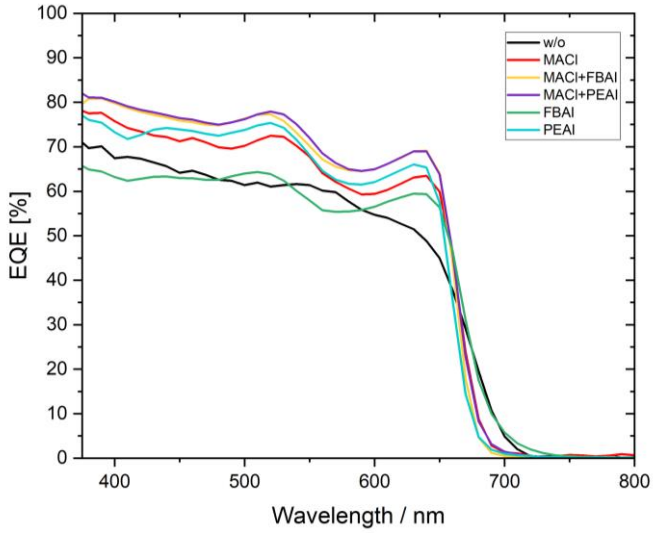

Figure 11: External quantum efficiency (EQE) of perovskite solar cells with different additives.

According to figure 11, the EQE could be increased upon addition of different additives. At about 650 nm, the highest EQE values with about 70 % was achieved for solar cells with MACl + FBAI and MACl + PEAI as additive, respectively. Like in I-V measurements, also here the effect of MACl as assisting additive for the formation of 3D/2D heterostructure perovskites can be deduced. Devices with FBAI and PEAI in absence of MACl show a significant lower EQE of 60 - 65 %. However, compared to devices without additives, having an EQE of roughly 50 % at 650 nm, all additives were able to increase the performance.

Another parameter that can be extracted from the EQE is the band gap. In table 9, the determined band gaps are listed.

Table 9: Experimentally determined band gap from external quantum efficiency of perovskite solar cells.

Composition	Band gap / eV
w/o	1.81
MACl	1.83
FBAI	1.82
PEAI	1.85
MACl+FBAI	1.84
MACl+PEAI	1.84

For the band gap determination, the squared product of photon energy and EQE was plotted against the energy in eV. Afterwards, a linear regression for the onset of the obtained curve was drawn. The intersection of the baseline with this linear fit gives then the band gap. [20] Supported by literature [21], for the deviations in the curves several reasons can be addressed. As EQE measurements are performed under normal atmosphere, degradation of the devices could affect the results. In order to check the reliability of the EQE measurement, the J_{SC} of EQE was compared to those of the I-V characterization in accordance to [21]. The $J_{SC\ EQE}$ can be calculated by following Eq. 4.

$$J_{SC\,EQE} = q \int_{\lambda_1}^{\lambda_2} EQE(\lambda)\ \Phi(\lambda)\ d\lambda \qquad (4)$$

The EQE of the device is multiplied with the photon flux Φ of the solar spectrum AM1.5G [22] and is integrated over the wavelength.[9]

In table 10, deviations in a range of -1.0 - 1.9 mA cm^{-2} are shown. This can be explained by the nature of the different experimental setup and the longer measurement times in case of EQE. Errors in the area determination or heating of the device under the intense light of the solar simulator during the I-V measurements can lead to deviations from EQE-determined currents. A positive delta Δ indicates, that J_{SC} of EQE measurements was higher than in I-V, while negative values show the opposite correlation.

Table 10: Comparison of the J_{SC} from external quantum efficiency measurements $J_{SC\ EQE}$ with $J_{SC\ IV}$ from current density - voltage measurements.

Composition	$J_{SC\ IV}$ / mA cm^{-2}	$J_{SC\ EQE}$ / mA cm^{-2}	Δ $J_{SC\ EQE-IV}$ / mA cm^{-2}
w/o	13.5	12.5	-1.0
MACl	13.6	13.0	-0.6
FBAI	11.2	12.9	+1.7
PEAI	11.2	13.1	+1.9
MACl + FBAI	12.3	13.3	+1.0
MACl + PEAI	12.1	13.5	+1.4

3.2. Maximum Power Point tracking (MPP)

For the MPP tracking, the devices were operated at maximum power point and the performance was measured over time. MPP tracking is used to investigate the long-time stability of a solar cell. During the measurement, the voltage at maximum power point V_{MPP} will

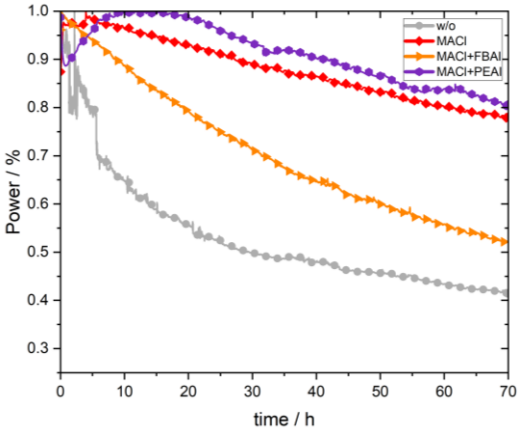

decrease due to aging of the device and degradation, caused by continuous illumination. As a consequence, also the power output of the device will lower over time. [23]

Figure 12: Stability determination of perovskite solar cells by Maximum power point (MPP) tracking.

Figure 12 shows a normalized plot of the recorded power over time. An increase in stability of the perovskite solar cells upon addition of additives can be derived. Devices with MACl and MACl + PEAI, respectively, showed relatively high stability. As a reference, t_{80} and t_{60}, the times until 80 % or 60 %, respectively, of the initial maximum power is reached, is listed in table 11.

Table 11: Stability results from maximum power point (MPP) tracking.

Composition	t_{80} / h	t_{60} / h
w/o	-	14
MACl	65	>70
MACl + FBAI	19	50
MACl + PEAI	>70	>70

For the perovskite solar cell without additive, an unusual drop in the recorded power can be seen in figure 12. This could possibly be due to a bad contact between the electrodes. In general, no exact qualitative information about the stability of the measured solar cells can be extracted from this data. MPP tracking is usually performed over a much longer period up to several hundred hours. [24] Furthermore, errors in measurement due to external factors cannot be excluded, as the setup was placed in a frequently used room. Change in the incident light intensity due to other light sources could have therefore affected the MPP measurements.

3.3. Transmittance

Transmittance measurement was performed with UV-Vis spectrometer, to obtain information about the change in absorption behaviour of the photoactive perovskite layer in dependence of different additives. One key parameter that is influencing the absorption coefficient of the perovskite material, and therefore affects the intensity of the spectral lines is the film thickness. In past research [25] it was reported, that with an decreasing film thickness, less light is absorbed. Referring to the conducted measurements in this thesis, this should be indicated by a higher transmittance, compared to devices with bigger film thickness. Film thickness of the diverse perovskite compositions were measured with Dektak profilometer on four different spots. Average values with standard deviation are summarized in table 12.

Table 12: Determined film thickness and standard deviation for perovskite solar cells.

Composition	Film thickness / nm
w/o	245 ± 5
MACl	253 ± 3
MACl+FBAI	234 ± 4
MACl+PEAI	236 ± 5
FBAI	241 ± 8
PEAI	247 ± 7

According to table 12, only marginal deviations in film thickness were measured. This is coherent with figure 13, as the recorded transmittance also shows no significant deviation.

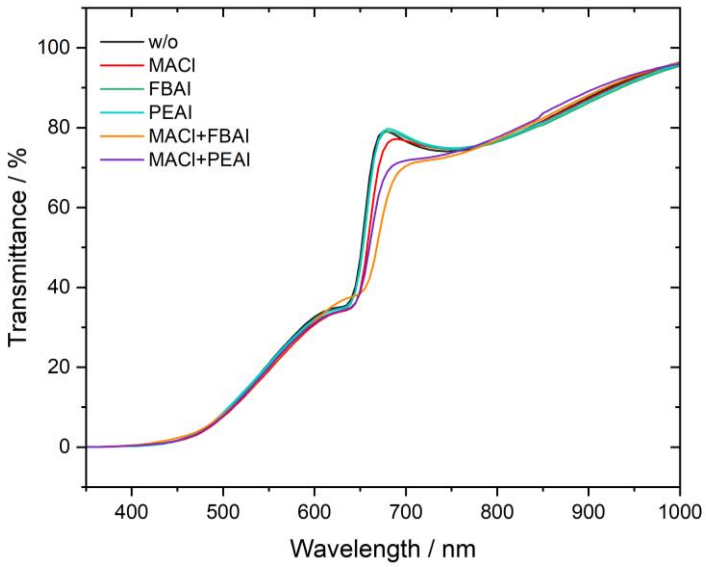

Figure 13: Transmittance spectrum for perovskite solar cells obtained from UV-Vis spectroscopy.

3.4. Steady-state Photoluminescence (PL)

PL spectroscopy is used as a method for determining imperfections in perovskite films, band gaps and halide segregation, that might be induced by photons. Figure 14 shows big deviations in the intensity for the varying perovskite composition. According to literature [26], the less deficiencies are present in the structure, the less possibilities for non-radiative charge recombination are given. Radiative charge recombination is then increased, which leads to a stronger light emitting species, and an increased signal in the PL measurement. [27] Therefore, the addition of FBAI and PEAI achieved the best passivation as they show the highest PL signals.

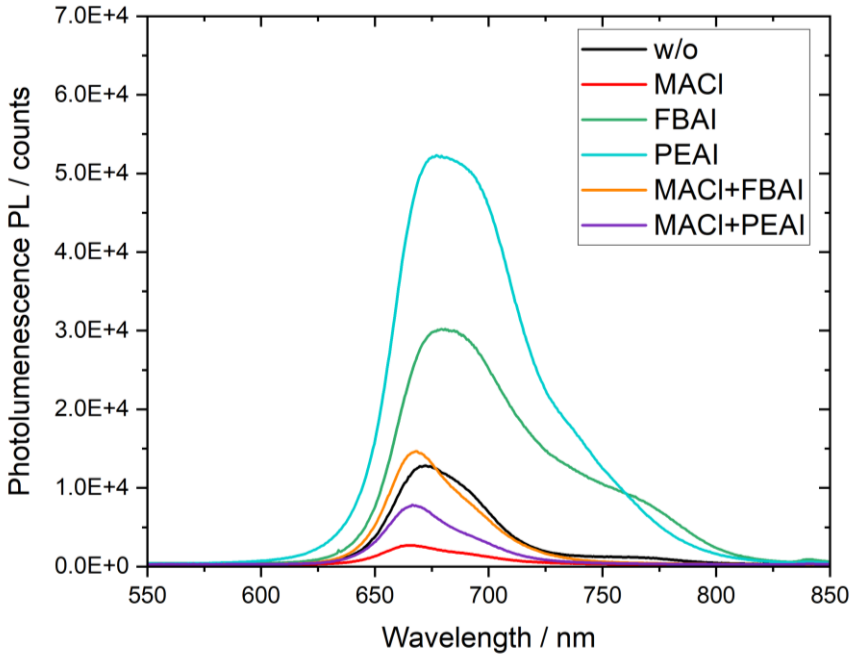

Figure 14: Photoluminescence (PL) measurement of perovskite solar cells.

The peaks are asymmetric towards higher wavelength. This could imply, that another emitting species is present when an additive is used, as this effect is most visible for perovskites including FBAI, MACl + FBAI and MACl + PEAI. Halide segregation could be another reason for the asymmetric peak shape. This is a frequently reported phenomenon especially for wide-band gap perovskites with a large iodide to bromide ratio. The two halides separate into different domains. While iodide segregates at lower band gap, bromide is preferring higher one. This leads to non-uniform optical properties and result in the specific peak shapes. [28] However, as results from MPP tracking show an increased lifetime for devices with FBAI, PEAI and MACl, the halide segregation is unlikely the main reason for the asymmetric peak shape.

3.5. Scanning Electron Microscopy (SEM)

To understand the influence of additives on the surface and grain boundaries of the perovskite SEM images were recorded. The images were recorded with a magnification factor of 8500 and 30000, respectively. Resolution is very limited, due to the very small grain size of approximately 500 – 1000 nm.

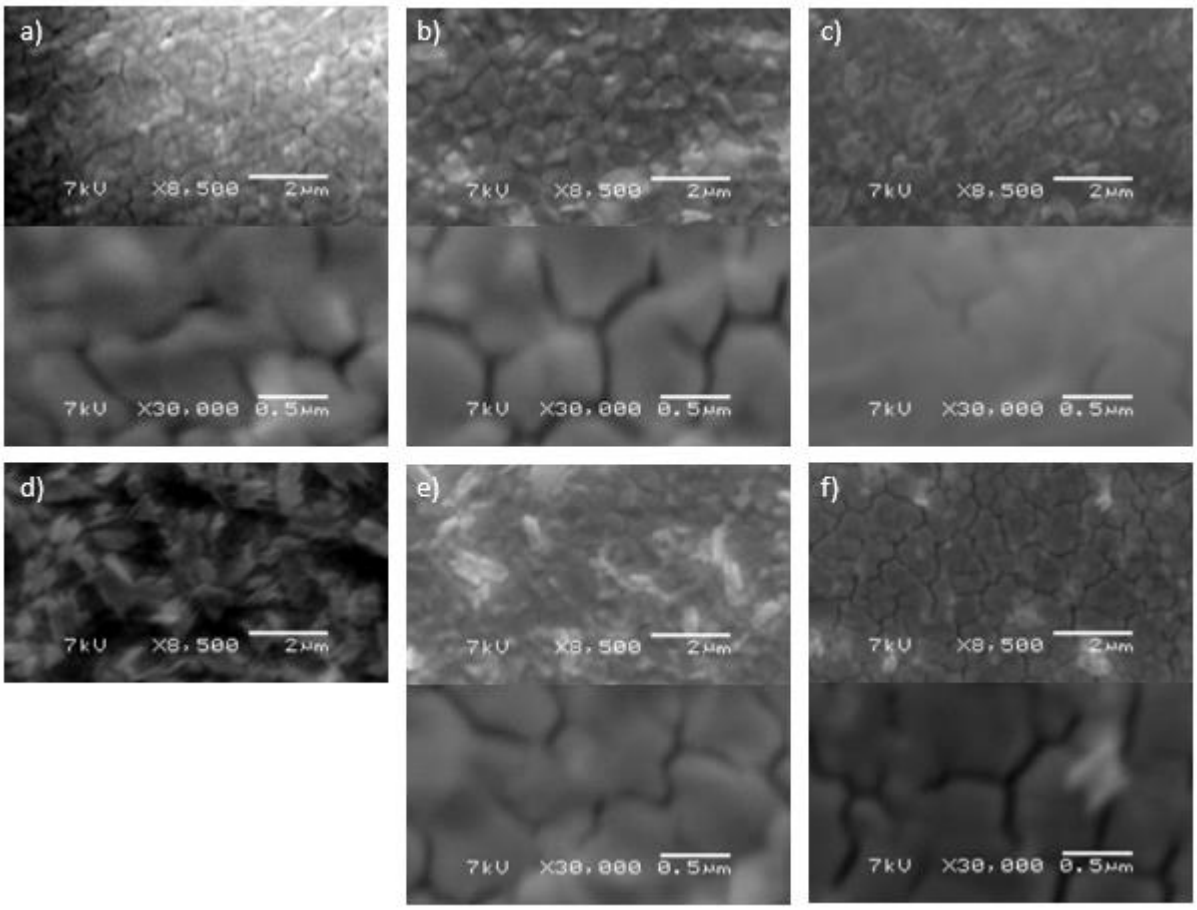

Figure 15: Scanning electron microscope images of the surface of perovskite solar cells with the composition **a)** w/o, **b)** MACl, **c)** FBAI, **d)** PEAI, **e)** MACl + FBAI, **f)** MACl + PEAI

According to figure 15b, MACl could slightly increase the grain size of the perovskite film, compared to devices with no additive. Hence, this can positively affect the charge transport and decreases defects in the material, as already mentioned in chapter 1.4. This could be a plausible reason for the increased V_{OC} and J_{SC} that can be extracted from figure 10 in the I-V measurements. Same trend for the grain size can be observed for the 3D/2D heterostructure perovskites with the composition MACl + FBAI and MACl + PEAI, according to figure 15e and 15f.

4. Conclusion and Outlook

In this thesis, the properties of 3D/2D heterostructure perovskites as photoactive layer in solar cell was investigated. I-V measurements showed that the additives MACl, FBAI and PEAI can increase the open circuit voltage, compared to solar cells without additive. The highest V_{OC} was achieved for the combination MACl + FBAI with 1.25 V on average. A comparison to the devices with FBAI alone (1.22 V) implies that MACl improved additionally the interface between the layers in the perovskite heterostructure. Considering the short circuit current, an opposite trend was obtained. This is as expected, as the applied additives have insulating properties and hinder the charge transport to the electrodes. Overall, the best power conversion efficiency was obtained for the 3D/2D heterostructure perovskite with MACl + FBAI as additive yielding an average PCE of 11.9 %. Long-time stability tests by maximum power point tracking revealed an increased stability of the perovskite films with implementation of the MACl in combination of FBAI and PEAI.

For further research, different methods for applying MACl and FBAI could be studied: Further optimization of the concentration and investigation of different processing parameters, including the spin coating of the thin layer and annealing processes, could lead to better performance. For future research it would be of interest, to find new methods to include FBAI and PEAI directly into the perovskite precursor solution, rather than processing as an extra thin layer. This could further improve the surface and prevent deficiencies in the perovskite bulk. Current and voltage would be therefore increased and could push the power conversion of 3D/2D heterostructure perovskites to even higher values.

5. References

[1] N. Kannan, D. Vakeesan, *Renewable and Sustainable Energy Reviews* **2016**, *62*, 1092 – 1105.

[2] Lucibella M., Chodos A, Johnson K., Bennet-Karaski N., *APS NEWS* **2009** *(18)*, 2.

[3] S. Philipps in ISE Fraunhofer "*Photovoltaics Report 2023*", URL: https://www.ise.fraunhofer.de/content/dam/ise/de/documents/publications/studies/Photovoltaics-Report.pdf (Accessed on September 17, 2023)

[4] M. I. H. Ansari, A. Qurashi, M. K. Nazeeruddin, *J. Photochem. Photobiol., C* **2018**, *35*, 1 – 24.

[5] *NREL* in "Best Research-Cell Efficiency Chart", URL: http://www.nrel.gov/ncpv/images/efficiency chart.jpg (Accessed on August 24, 2023)

[6] Di Zhou, T. Zhou, Y. Tian, X. Zhu, Y. Tu, *J. Nanomater.* **2018**, 1 – 15.

[7] T. Hellmann, C. Das, T. Abzieher, J. A. Schwenzer, M. Wussler, R. Dachauer, U. W. Paetzold, W. Jaegermann, T. Mayer, *Adv. Energy Mater.* **2020**, *10 (42)*, 2002129.

[8] N. Kaminski, in "State of the art and the future of wide band-gap devices.", Thesis University of Bremen, **2009**

[9] K. Gugujonović, F. Mayr, B. Hailegnaw, S. Pöllner, R. Zahrhuber, A. Planer, C.-H. Wang, C.-S. Hsu, M. C. Scharber, *Monatsh Chem*, in press.

[10] N. Marinova, S. Valero, J. L. Delgado, *J. Colloid Interface Sci.* **2017**, *488*, 373 – 389.

[11] M. Diantoro, T. Suprayogi, A. Hidayat, A. Taufiq, A. Fuad, R. Suryana, *Int. J. Photoenergy* **2018**, 1 – 7.

[12] L. Cojocaru, S. Uchida, K. Tamaki, P. V. V. Jayaweera, S. Kaneko, J. Nakazaki, T. Kubo, H. Segawa, *Scientific reports* **2017**, *7 (1)*, 11790.

[13] B. Chen, P. N. Rudd, S. Yang, Y. Yuan, J. Huang, *Chem. Soc. Rev.* **2019**, *48 (14)*, 3842 – 3867.

[14] R. Zhao, L. Xie, R. Zhuang, T. Wu, R. Zhao, L. Wang, L. Sun, Y. Hua, *ACS Energy Lett.* **2021**, *6 (12)*, 4209 – 4219.

[15] F. Zheng, C. Zuo, M. Niu, C. Zhou, S. J. Bradley, C. R. Hall, W. Xu, X. Wen, X. Hao, M. Gao, T. A. Smith, K. P. Ghiggino, *ACS Appl. Mater. Interfaces* **2020**, *12 (23)*, 25980 – 25990.

[16] X. Chen, H. Zhou, H. Wang, *Frontiers in chemistry* **2021**, *9*, 715157.

[17] T. Campos, P. Dally, S. Gbegnon, A. Blaizot, G. Trippé-Allard, M. Provost, M. Bouttemy, A. Duchatelet, D. Garrot, J. Rousset, E. Deleporte, *J. Phys. Chem. C* **2022**, *126 (31)*, 13527 – 13538.

[18] J. Herterich, C. Baretzky, M. Unmüssig, C. Maheu, N. Glissmann, J. Gutekunst, G. Loukeris, T. Mayer, M. Kohlstädt, J. P. Hofmann, U. Würfel, *Sol. RRL* **2022**, *6 (7)*, 2200195.

[19] P. Hierrezuelo-Cardet, A. F. Palechor-Ocampo, J. Caram, F. Ventosinos, D. Pérez-del-Rey, H. J. Bolink, J. A. Schmidt, *Journal of Applied Physics* **2020**, *127 (23)*, 235501.

[20] R. Carron, C. Andres, E. Avancini, T. Feurer, S. Nishiwaki, S. Pisoni, F. Fu, M. Lingg, Y. E. Romanyuk, S. Buecheler, A. N. Tiwari, *Thin Solid Films* **2019**, *669*, 482 – 486.

[21] M. Saliba, L. Etgar, *ACS Energy Lett.* **2020**, *5 (9)*, 2886 – 2888.

[22] *NREL* in “Reference Air Mass 1.5 Spectra”, URL: https://www.nrel.gov/grid/solar-resource/spectra-am1.5.html. (Accessed on August 24, 2023)

[23] Rabindra Satpathy, Venkateswarlu Pamuru, in *Solar PV Power* (Eds: Rabindra Satpathy, Venkateswarlu Pamuru), Academic Press **2021**.

[24] M. Saliba, M. Stolterfoht, C. M. Wolff, D. Neher, A. Abate, *Joule* **2018**, *2 (6)*, 1019 – 1024.

[25] C. Roldán-Carmona, O. Malinkiewicz, R. Betancur, G. Longo, C. Momblona, F. Jaramillo, L. Camacho, H. J. Bolink, *Energy Environ. Sci.* **2014**, *7 (9)*, 2968 – 2973.

[26] V. Campanari, F. Martelli, A. Agresti, S. Pescetelli, N. Y. Nia, F. Di Giacomo, D. Catone, P. O'Keeffe, S. Turchini, B. Yang, J. Suo, A. Hagfeldt, A. Di Carlo, *Sol. RRL* **2022**, *6 (8)*, 2200049.

[27] M. Stolterfoht, V. M. Le Corre, M. Feuerstein, P. Caprioglio, L. J. A. Koster, D. Neher, *ACS Energy Lett.* **2019**, *4 (12)*, 2887 – 2892.

[28] J. Liang, C. Chen, X. Hu, Z. Chen, X. Zheng, J. Li, H. Wang, F. Ye, M. Xiao, Z. Lu, Y. Xu, S. Zhang, R. Yu, C. Tao, G. Fang, *ACS Appl. Mater. Interfaces* **2020**, *12 (43)*, 48458 – 48466.